Renewable Energy 143 (2019) 390–403

Contents lists available at ScienceDirect

Renewable Energy

journal homepage: www.elsevier.com/locate/renene

The trade-off between tidal-turbine array yield and environmental impact: A habitat suitability modelling approach

R.J. du Feu [a, b, *], S.W. Funke [c], S.C. Kramer [a], J. Hill [d], M.D. Piggott [a, b]

[a] Department of Earth Science and Engineering, Imperial College London, London, UK
[b] Grantham Institute, Imperial College London, London, UK
[c] Scientific Computing Department, Simula Research Laboratory, Oslo, Norway
[d] Department of Environment and Geography, University of York, UK

ARTICLE INFO

Article history:
Received 12 January 2018
Received in revised form
3 April 2019
Accepted 25 April 2019
Available online 4 May 2019

Keywords:
Marine renewable energy
Tidal turbines
Maximum entropy modelling
Multi-objective optimisation
Habitat suitability
Environmental impact

ABSTRACT

In the drive towards a carbon-free society, tidal energy has the potential to become a valuable part of the UK energy supply. Developments are subject to intense scrutiny, and potential environmental impacts must be assessed. Unfortunately many of these impacts are still poorly understood, including the implications that come with altering the hydrodynamics. Here, methods are proposed to quantify ecological impact and to incorporate its minimisation into the array design process. Four tidal developments in the Pentland Firth are modelled with the array optimisation tool OpenTidalFarm, that designs arrays to generate the maximum possible profit. Maximum entropy modelling is used to create habitat suitability maps for species that respond to changes in bed-shear stress. Changes in habitat suitability caused by an altered tidal regime are assessed. OpenTidalFarm is adapted to simultaneously optimise array design to maximise both this habitat suitability and to maximise the profit of the array. The problem is thus posed as a multi-objective optimisation problem, and a set of Pareto solutions found, allowing trade-offs between these two objectives to be identified. The methods proposed generate array designs that have reduced negative impact, or even positive impact, on the habitat suitability of specific species or habitats of interest.

1. Introduction

The United Kingdom contains a large proportion of the European tidal resource [1,2]. This is not just a consequence of its extensive coastline, but in particular of its unique position between a shallow shelf sea, the North Sea, and a deep ocean, the Atlantic Ocean. With every tidal cycle, vast quantities of water are pumped between these two bodies along the channels at the north and south of the mainland, the Pentland Firth and the English Channel. High tidal currents are then further accelerated around the local coastline and bathymetry features. These currents are ideal for generating power; Indeed the resource of the Pentland Firth is vast [3,4] and as such, it is the basis of much research. Such uniqueness, the very reason we want to exploit these regions, also fuels concern of what environmental effects such exploitation could have [5–7].

A tidal-turbine array can both slow down currents, through the very nature of energy extraction, and speed up currents, through the diversion of water around turbines and around the array itself. The micro-siting of turbines within an array is already considered as an integral part of array design, and research has demonstrated a great effect on the total energy extracted [8,9], but micro-siting is also a factor in determining the effect of the array as a whole upon local hydrodynamics. Therefore, the magnitude and manner of an array's effect on its environment can be said to be dependent on both its size and its design.

Both the production of power and the generation of profit from tidal turbine arrays have been heavily studied [10–13], and array design optimisation techniques have been developed that seek to maximise these objectives [14]. Similarly, the potential effects of an array upon its environment have been considered [15–17], and models developed to try and quantify such effects [5,18,19]. However, the interaction between these two outcomes is covered little in the literature. In fact, a study by van der Molen et al. [20] is, to the authors' knowledge at the time of writing, the only published paper that explicitly models the effect of tidal development on the marine

* Corresponding author. Department of Earth Science and Engineering, Imperial College London, London, UK
E-mail address: r.du-feu14@imperial.ac.uk (R.J. du Feu).

https://doi.org/10.1016/j.renene.2019.04.141
0960-1481/

ecosystem, using a biogeochemistry model to measure changes in the ecosystem for two different levels of tidal development. The methodology presented in this paper directly models the effect of tidal development on specific species or their habitat, seen only twice before in the context of theses [15,21]. This is, therefore, a very early attempt in which higher taxa are modelled explicitly, and in which the environmental impacts of tidal development on these taxa are quantified in a statistical framework, and the first such attempt in which this is done in an array optimisation context, and effects are not only quantified but mitigated for. The problem is posed as a multi-objective optimisation problem which seeks to maximise both profit generation as well as the area of suitable habitat of specific species. This approach is investigated using the framework proposed by du Feu et al. [22], which easily allows any trade-off to be thoroughly explored.

MaxEnt [23] is an open-source habitat suitability model that is used to produce maps of the occurrence probability of a species. OpenTidalFarm [24] is an open-source tidal-turbine array optimisation tool that determines optimal array size and layout to generate the maximum possible profit over the lifetime of the array. The methodology of MaxEnt has been reproduced here within OpenTidalFarm, allowing OpenTidalFarm to design arrays that are maximised for profit as well as for the habitat suitability of a specific species. These two objectives are weighted against each other, and the interaction between them is investigated through altering the weighting to find a range of possible solutions, all of which belong to the Pareto set of the multi-objective optimisation problem posed.

This approach is demonstrated in two test scenarios in the Pentland Firth. Four turbine farms are optimised simultaneously for profit and for the habitat suitability of one of two selected species, the acorn barnacle (*Balanus crenatus*) and the brown crab (*Cancer pagurus*). These species are chosen as they each react differently to the presence of the turbine farms, with *Balanus crenatus* tending to react negatively to reductions in bed shear stress and *Cancer pagurus* tending to react positively, although both relationships are dependent upon other variables than bed shear as well. Beyond this they both have a great abundance of available data, allowing for easy demonstration of the method. For each test case, a set of Pareto solutions of the multi-objective optimisation problem posed is found, and the Pareto front is visualised. This gives an understanding of the relationship between the two goals, and any trade-offs that exist between them can be identified. These two test cases are used to show that the techniques presented here can be used to design arrays that preserve or even improve habitat for species or habitat of importance.

2. OpenTidalFarm

2.1. The problem

OpenTidalFarm, as developed by Funke et al. [8,25], optimises tidal-array formation to maximise the profit generated by the array. In the configuration employed for this work turbines are not resolved individually, but instead the entire array is represented by a continuous turbine-density function, that scales linearly with a continuous friction function. OpenTidalFarm solves a problem of the following form, over a domain Ω:

$$\begin{aligned} &\max_{d} \ \text{Profit}(\mathbf{z}(d), d) \\ &\text{s.t. } F(\mathbf{z}) = 0, \\ &0 \le d \le \overline{d}, \end{aligned} \tag{1}$$

where $d : \Omega_{\text{farm}} \subset \Omega \to \mathbb{R}$ is the turbine density function that represents an array of tidal turbines of spatially varying configuration within the farm domain Ω_{farm}. $\mathbf{z} = (\mathbf{u}(d), \eta(d))$ is the solution to F, the depth-averaged shallow water equations, where $\mathbf{u} : \Omega \to \mathbb{R}^2$ is the depth-averaged velocity, $\eta : \Omega \to \mathbb{R}$ is the free-surface displacement. $\overline{d}$ is a user defined upper bound on turbine density, specifying the maximum number of turbines allowed per unit area.

Representing the farm in this way, using a single continuous turbine density function as opposed to a priori specifying a number of turbines and modelling them discretely, allows both the optimal size of the farm and the spatial layout of the turbines to be found simultaneously, while also allowing coarser meshes to be used resulting in each flow solve being computationally cheaper. After the turbine density function, d, is found, the optimal number of turbines in the farm, N, can be calculated by integrating the optimised density function over the domain:

$$N = \int_{\Omega} d(x)\, dx. \tag{2}$$

The profit functional used by OpenTidalFarm is a function of both the revenue produced by the farm and the cost of the farm. The revenue is assumed to scale linearly with the energy extracted while the cost model used is simple, being based only on the total number of turbines, calculated as defined above. Cost models that incorporate the price of cabling into a separate configuration, in which turbines are realised discretely, have been developed [26], and more complex cost models are the subject of future work. Profit is expressed as

$$\begin{aligned} &\text{Profit}(d) = \text{Revenue}(d) - \text{Cost}(d), \\ &\text{Revenue}(d) = IkE(d), \\ &\text{Cost}(d) = cN, \end{aligned} \tag{3}$$

where I denotes the income generated per unit energy, $0 \le k \le 1$ is a turbine efficiency coefficient that represents loss of energy, $E(d) = E(\mathbf{z}(d), d)$ is the energy extracted from the flow $\mathbf{z}$, and c is the cost associated with each turbine.

To formulate this as a maximisation problem Funke et al. [25] divide through by IkL where L is the lifetime of the farm. The energy term becomes one of average power, P, and the cost is then measured in terms of the energy that could be bought for that cost, which is spread across the lifetime of the farm, so both terms are measured in Watts and can be optimised for simultaneously. The profit functional then becomes

$$\text{Profit}(d) = \frac{E(d)}{L} - \frac{cN}{LIk}. \tag{4}$$

An estimation for the cost term $c/(LIk)$ is outlined by Funke et al. [25], as is a full derivation of the OpenTidalFarm methodology [8].

OpenTidalFarm can be run on either a steady-state, time-independent problem or on a time-dependent one, over a user-specified period. For simplicity over the interpretation of the result, and to reduce overall computational times, we consider only the steady-state problem, replicating conditions at peak flood flow. Running on such a steady-state model results in the assumption that energy production would be at peak levels throughout the entire lifetime of the farm, which results in artificially high values for power and profit. If using this method to make real decisions on array design a time-dependent model that covers at least an entire tidal cycle should be used, but for the purposes of demonstrating the method a steady-state model is sufficient.

2.2. The optimisation process

OpenTidalFarm uses a gradient-based optimisation algorithm to

solve a discretised version of the problem [8]. The hydrodynamic flow field produced in the presence of the turbine array is evaluated at each iteration through solving the steady-state shallow-water equations using the finite-element method. The functional of interest, Profit, is evaluated from this solution, and the gradient of Profit with respect to the turbine density function is calculated by solving the adjoint shallow-water equations. If the optimisation criteria are satisfied then the algorithm terminates at this stage. These criteria include the convergence of the gradient or the surpassing of a set number of iterations. If the criteria have not been satisfied then the turbine density, d, is updated and the process is repeated until the optimisation criteria are met. The complete methodology and justification for OpenTidalFarm optimisation is outlined in detail by Funke et al. [8,25].

Gradient-based optimisation is necessary due to the small iteration numbers required compared to gradient-free approaches. This allows for the use of a fully coupled shallow-water model that calculates the resultant flow in the presence of the array. This is imperative when investigating the interaction between an array and its environment, and especially so with large-scale arrays where blockage effects become significant [27]. There is always, however, the disadvantage that with gradient-based optimisation solutions are not guaranteed to be global optima, but local optima only. A previous study by du Feu et al. [22] found that despite this limitation, the method used here is effective in finding the Pareto Front to the multi-objective optimisation problem posed and that the solutions found consistently lie close to or on the Pareto front. Other studies instead employ genetic algorithms to find optimal array formations, for example, Bilbao and Alba [28] who optimised an array of 47 turbines with 61,802 model evaluations. Even here global optima are not always guaranteed, and beyond this in such scenarios, due to the large iteration numbers required, much cheaper hydrodynamic models have to be used.

3. Creating the habitat functional

3.1. Habitat suitability modelling

In order to create a functional that allows OpenTidalFarm to minimise potential damage to habitat, habitat must be expressed mathematically so that it can be quantified. Habitat suitability modelling is used to do this. A habitat suitability model estimates the probability of occurrence of a species across a spatial domain using species occurrence records and environmental data [29]. Correlations are then found between a species and the environmental conditions in which it is, or is not, found. These correlations can then be used to judge the suitability of any habitat in housing that species. For example, this paper looks at the barnacle *Balanus crenatus*, that is expected to like high energy environments with high bed shear stress levels (a common habitat preference for barnacle species [30,31]), and the crab *Cancer paragus* that is expected to like lower energy environments [32,33]. The recent growth in the use and understanding of such modelling has been driven by the rise in the availability of open-access forms for both of these data, for example the National Biodiversity Network (NBN) [34] which was founded in 2000 and collates data from a multitude of different agencies and organisations, and is considered as one of the best repositories for such data, containing records for over 127 million species.

Habitat suitability models can either require both species presence and absence data or species presence data only. Presence-absence models generally outperform presence-only models, but reliable presence-absence data is very hard to come by while presence data is often abundant and freely available, hence the rising popularity of presence-only models. MaxEnt [29] is a presence only model and is the habitat suitability model used here. MaxEnt was chosen due to its availability, the extensive literature on its methodology and use [35–39], its concise mathematical definition, allowing it to be replicated within OpenTidalFarm (section 3.2), and its record of performance. MaxEnt has been shown to perform as well as other presence-only species distribution models [40], while significantly outperforming some [41]. One study [42] compared MaxEnt to one other presence-only model, and to two presence-absence models. MaxEnt not only outperformed the other presence-only model but, for three of the four test cases considered, exhibited no significant difference in performance to the presence-absence models.

MaxEnt estimates the unknown probability distribution, $\pi(x) : X \to \mathbb{R}^+$ where $\sum_{x \in X} \pi(x) = 1$, that describes the likelihood of finding a certain species across a set of discrete grid cells X, representing a geographic domain Ω. It does this using a sample set of species occurrences, $x_1, \ldots x_m \in X$, and a set of *features*, $f_1, \ldots, f_n : X \to \mathbb{R}$ that describe environmental variables. These environmental variables can be continuous, such as average temperature or water depth, in which case they need to be converted to fit onto the domain X, or they can be categorical, such as substrate type. The features themselves can either represent the raw environmental variables or higher level functions of those variables, such as quadratics, products and threshold functions. For a full explanation of the different feature types see Phillips et al. [35]. π is characterised by the expected values of the features, which are estimated using the expected value of each feature across the sample set of known species occurrences. That is, the expected value of a feature under π is

$$\pi\left[f_j\right] = \sum_{x \in X} \pi(x) f_j(x) = \tilde{\pi}\left[f_j\right] = \frac{1}{m} \sum_{i=1}^{m} f_j(x_i), \tag{5}$$

where $\tilde{\pi}$ is the uniform distribution across the sample points. MaxEnt considers all such distributions π and selects the distribution closest to uniform, of maximum entropy, uniquely determining a species occurrence distribution for the chosen species [43].

It has been shown that the chosen $\pi(x)$ is equivalent to the Gibbs distribution $q_\lambda(x)$ that maximises the likelihood of the sample set, $\Pi_{i=1}^{m} q_\lambda(x_i)$ [43]. That is, $\pi(x)$ is equivalent to

$$\begin{aligned} q_\lambda(x) &= \frac{e^{\lambda \cdot f(x)}}{Z_\lambda}, \\ \text{s.t. } \lambda &= \min_{\lambda} \left| \ln(Z_\lambda) - \frac{1}{m} \sum_{i=1}^{m} \lambda \cdot f(x_i) \right|, \end{aligned} \tag{6}$$

where Z_λ is a normalisation constant that ensures that the Gibbs distribution sums to 1.

When expressed as a Gibbs distribution, the model is uniquely characterised by λ which contains information on the importance of each feature in determining the final distribution. That is, it defines the relationship between the chosen set of environmental variables and the habitat suitability of the chosen species. This vector is output by MaxEnt and can be used to create distributions of occurrence probability under different conditions. For example, for a different domain, or under a change in the environmental variables, such as a change in flow regime given the presence of a tidal-turbine array. Once the Gibbs distribution has been calculated it undergoes a logistic transform to produce an output that estimates the probability of a species being present at each point in the domain, returning a value between 0 and 1 for each point. For full details on the MaxEnt methodology see Phillips et al. [29,35].

3.2. Integrating OpenTidalFarm and MaxEnt

A habitat functional, H, is introduced into OpenTidalFarm, defined as the integral of the Gibbs distribution across the chosen domain, Ω. This allows the habitat suitability of the domain to be expressed as a single quantifiable number and allows OpenTidalFarm to calculate both habitat suitability and profit at each iteration, and optimise for both simultaneously. H is defined as so that the value of H for an array represented by the turbine density function, d, is calculated using the state of each feature under the present flow solution, $\mathbf{u}(\mathbf{z}; d)$, that is determined by the turbine density function. In order to use this functional for a specific species, the vector λ must first be obtained. Initially, a shallow-water hydrodynamic model is run without the presence of any turbines in order to obtain the ambient flow regime and provide information that can be used to create the environmental variables that MaxEnt requires.

$$H(d(\mathbf{z})) = \int_{\Omega} \frac{e^{\lambda \cdot f(\mathbf{u}(\mathbf{z};d))}}{Z_{\lambda}}\, dx, \tag{7}$$

A MaxEnt model is built as described in section 3. Species occurrence data is obtained from the NBN, and the following environmental variables are used as features:

1. Depth [m]: this is taken from the bathymetry data for the hydrodynamic model.
2. Substrate type: this is taken from the European Marine Observation and Data Network [44] who hold data on substrate type of the seabed in Europe, using the EUNIS classification system [45] to identify the seabed as either 'hard substrata' or 'soft substrata'.
3. Distance to shore [m]: this is calculated from the domain of the hydrodynamic model, using the Eikonal equation to find the shortest distance between each point and any closed boundary.
4. $|\mathbf{u}|$[m s^{-1}]: the flow speed at each point, taken from the hydrodynamic model.
5. τ [Pa]: the bed shear stress magnitude at each point, taken from the hydrodynamic model.

As MaxEnt uses a discrete domain and OpenTidalFarm uses a continuous domain, the continuous variables output from the shallow-water model are converted into discrete variables over the grid domain of the MaxEnt model. This is done by taking, from the results of the shallow-water model, the value at the centre of each grid square as defined by the MaxEnt grid domain. The MaxEnt domain is chosen to match the smallest mesh resolution from the shallow-water model in order to avoid missing information from any of the mesh cells. Bed shear stress magnitude is defined as

$$\tau = \rho C_d |\mathbf{u}|^2, \tag{8}$$

where $\rho = 1000$ kg m^{-3} is the density of seawater and C_d is the drag coefficient of the seabed.

The vector λ is output by MaxEnt and read into OpenTidalFarm. This allows the species occurrence distribution to be modelled at each iteration after the hydrodynamic model is solved with the updated turbine friction function, d. Each feature defined by the MaxEnt model is recreated as a continuous function on the domain of the hydrodynamic model, Ω, using the results of the model. These features will then be updated at every iteration with the updated density function d, and the updated flow regime. The Gibbs distribution is calculated using these updated features and the known and fixed vector λ, giving the habitat functional, H.

3.3. Final problem formulation

The final problem formulation is

$$\begin{aligned}
&\max_{d} \omega_p \mathrm{P}(d) + \omega_h \mathrm{H}(d),\\
&\mathrm{P}(d) = \frac{1}{L} E(\mathbf{z}, d) - \frac{c}{LIk} \int_{\Omega} d(x)\, dx,\\
&\mathrm{H}(d) = \int_{\Omega} \frac{e^{\lambda \cdot f(x)}}{Z_{\lambda}}\, dx,\\
&\text{s.t.} F(\mathbf{z}) = 0,\\
&0 \le d \le \overline{d},\\
&\omega_p + \omega_h = 1,
\end{aligned} \tag{9}$$

where ω_p and ω_h are the weights of P and H respectively, and all other symbols are as in section 2.1. This represents a linear scalarisation of the multi-objective optimisation problem [46] of maximising the non-comparable objectives of P and H, and will return a single solution on the Pareto front of that problem.

By altering the weight of each functional, different Pareto solutions can be found [46], and by running a series of optimisations of different weights, the Pareto front can be uncovered. The two weights are combined into a single variable termed *importance*, ι, that expresses the weight of the habitat functional relative to the profit functional. An optimisation of $\iota = 0$ optimises for P only, and as ι is increased more weight is placed on H. This allows for easy exploration of the most interesting section of the Pareto front, as demonstrated by du Feu et al. [22].

The weights themselves represent the societal importance placed on the respective objectives, and the Pareto front represents all optimal options of compromise between fulfilling those two objectives. The 'best' solution can only be identified by the stakeholders in the tidal array under construction, who would have to decide the importance they are willing to place upon each objective. If the Pareto front can be found the stakeholders will have information that could be vital in making such a decision.

4. Creating the test cases

4.1. The hydrodynamic model

The habitat functional is tested on a large steady-state shallow water model of the Pentland Firth, Fig. 1. The Pentland Firth is a large channel that lies between the north coast of Scotland and the Orkney Isles. It is divided by two main islands: Swona, in the north, and Stroma, in the south. There are four areas within the Pentland Firth that have been leased by the crown estate for commercial tidal-power development [47]. These are 1) Cantick Head, 2) Inner Sound of Stroma, 3) Ness of Duncansby, and 4) Brough Ness. The mesh used for the model included the entire area of the Firth and consisted of 321,224 elements which ranged in size from 100 m to 350 m. The finest mesh resolution was only used within the farm domains themselves, with the mesh getting gradually coarser outside of these areas. For background on the mesh generation process refer to Avdis et al. [48]. The domain was given a realistic bathymetry using data collated from four different sources: 1) the global bathymetry dataset GEBCO_08 [49], 2) Digimap [50], 3) the Scottish Government [51] and 4) data obtained from MeyGen. This is the same mesh and the same bathymetry data as used by Funke et al. [25]. The cost coefficient, which represents the power equivalent of the cost of a turbine, was estimated at 1628 kW

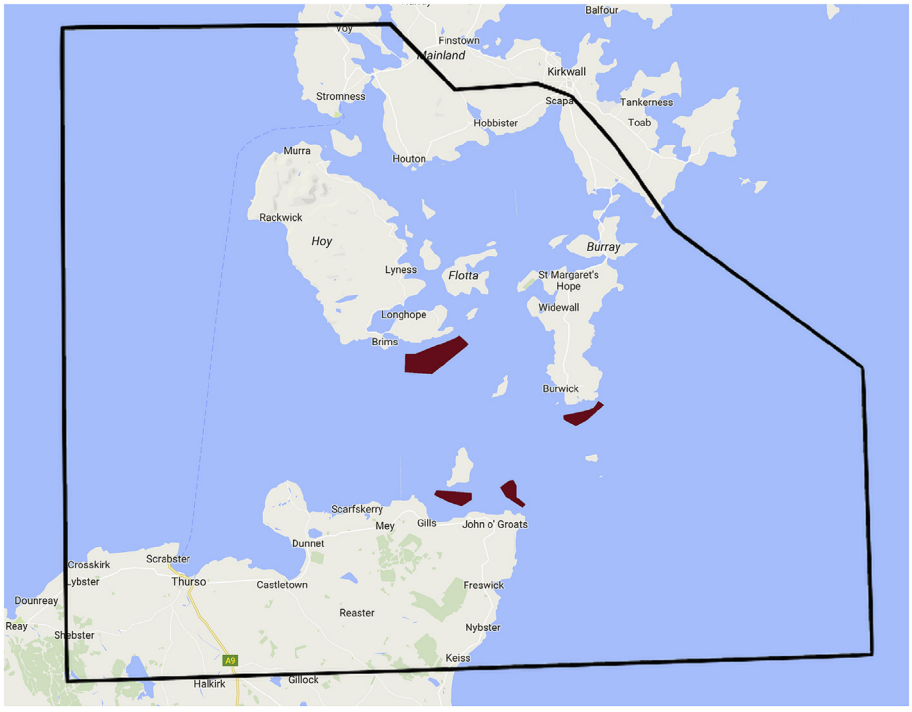

Fig. 1. The domain of the hydrodynamic model, the Pentland Firth at the North East of the Scottish mainland, approximately 68 km by 54 km. (Google Maps, Google). The boundaries of the model are marked in black, and the four tidal farms are marked in red. 1) Cantick Head, 2) Inner Sound of Stroma, 3) Ness of Duncansby, and 4) Brough Ness. (For interpretation of the references to colour in this figure legend, the reader is referred to the Web version of this article.)

following Funke et al. [25]. This cost model does not include various costs such as cabling and maintenance, so could be an underestimation that would result in artificially high numbers of turbines.

The coastal boundaries are subject to a free-slip condition, while the ocean boundaries are open. The model is forced with a constant inflow of $2 m \cdot s^{-1}$ from the western boundary and the free-surface displacement is set to zero on the eastern boundary. This approximates the conditions of peak flood flow, the point in the tidal cycle where the flow velocity is at a maximum, showing similar flow speeds and tidal structures to other models [25,52]. To achieve convergence, the viscosity was set to 100 $m^2\ s^{-1}$ in the body of the domain, and to remove instabilities at the open boundaries viscosity was set to 1000 $m^2\ s^{-1}$ within a 1 km band around each boundary. The forward model was run without the presence of a turbine array, and the ambient flow regime was stored.

4.2. The MaxEnt model

A MaxEnt model is built, as described in section 3, with a mesh resolution of 100 m, using the five environmental variables (Fig. 2) of depth, substrate type, distance to shore, flow velocity and bed shear stress. The bed shear stress coefficient, C_d, for the Pentland Firth was taken to be 0.005, based on work by Baston and Harris [53], and Easton and Woolf [54].

It is important to note at this point that the hydrodynamic model used here is a steady-state model, and not a time-dependent model, while the sampling data is real so is of course based on the real tidal regime. However, benthic assemblages tend to adapt to the greatest forces they experience through a tidal cycle [55], as opposed to average forces. For example, Bell et al. in 2011 considered only maximum, not average, values for bed shear stress and current shear stress in their MaxEnt model that was looking into effects of wave and tidal energy on marine organisms [56], while Harendza [15] removed average bed shear stress as a variable, retaining only maximum bed shear stress, after concluding that the average values were not important in determining habitat suitability for a range of different species. Therefore, environmental variables that capture only the maximum forces experienced throughout the tidal cycle are deemed sufficient for the purposes of this work. There is still the caveat that these forces, experienced here during peak flood, cannot be fully captured using only a steady state model. The size of the domain and the resulting phase difference will create a consistent difference to the true peak flood, so artificial correlations may arise with the sampling data. However, the method presented is still sound, and the results valid as a proof-of-concept of the general approach, which remains the first attempt to quantify the ecological impact of tidal-turbine farms for higher taxa.

Two species are selected for use as test cases, *Balanus crenatus* (the acorn barnacle) and *Cancer pagurus* (the brown crab), and their species occurrence data are obtained from the National Biodiversity Network [34]. These species are chosen to demonstrate the methodology introduced in this paper due to the sufficient level of presence data available, due to MaxEnt models that perform well, and because they display different habitat preferences to each other (Fig. 3).

In both cases, the most important feature in determining habitat suitability is the distance to shore, followed by the bed shear stress, with depth also having importance. For both species it is advantageous to be close to shore, however, for bed-shear stress, the relationships are different (Fig. 4). *Balanus crenatus* displays a positive correlation with bed shear stress, with habitat suitability rising as bed shear stress rises (Fig. 4 (b)). Conversely, *Cancer pagurus* displays a negative correlation with the square of the flow velocity, which is analogous to the bed shear stress (Fig. 4 (e)). The inextricably linked nature of flow velocity and bed shear stress means that MaxEnt may, as in this case, pick up on the importance of the square of the velocity variable instead of placing importance

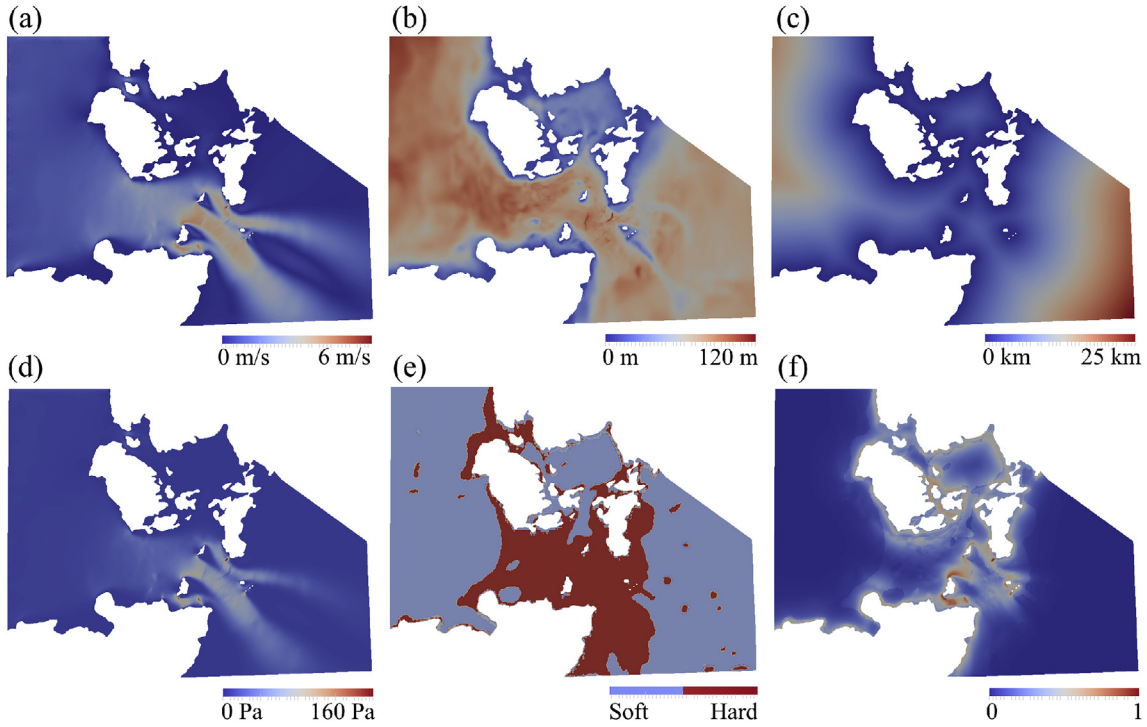

Fig. 2. The environmental variables used in the MaxEnt model: (a) flow velocity, (b) depth, (c) distance to shore, (d) bed shear stress and (e) hard or soft substrate type. (f) shows an example habitat suitability map as produced by the maximum entropy model, showing species occurrence likelihood for *Balanus crenatus*, here created within OpenTidalFarm as described in section 3.2.

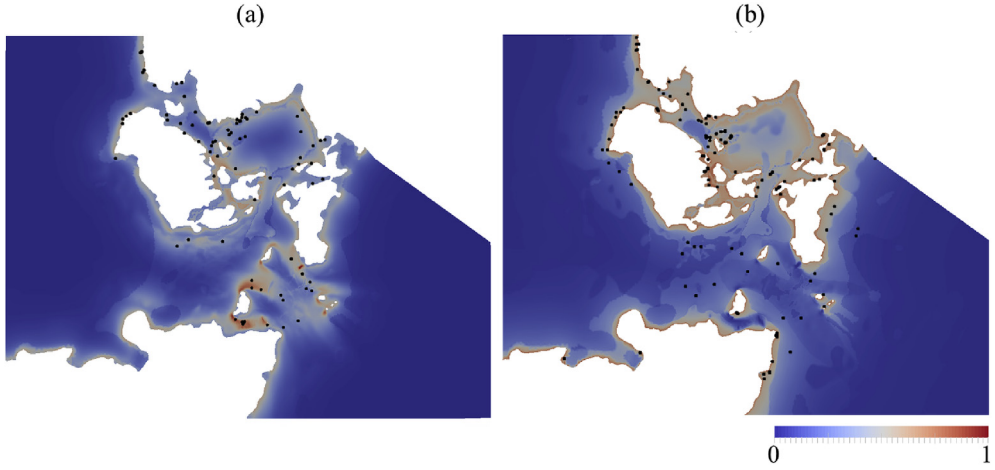

Fig. 3. Habitat suitability maps for the two species selected for use as test cases, (a) *Balanus crenatus* and (b) *Cancer pagurus*. Species occurrence records [34] are marked in black.

directly on the bed shear stress variable. This does not cause a problem as the relationship is still captured, and is unavoidable as neither of these variables can be removed from the model without losing potential information on the relationships between them and other variables. The results of these MaxEnt models suggest that *Balanus crenatus* will largely respond negatively to the reduction of flow caused by the turbine farms, whereas *Cancer pagurus* will largely respond positively. Graphs such as those in Fig. 4 should be treated with caution, as they do not fully capture the relationships between features within MaxEnt. For example, the relationships that were seen with *Cancer pagurus* between the depth and both the bed shear stress and the flow velocity, that tell us that it is expected to respond differently to changes in the flow at different depths.

The quality of the MaxEnt models is assessed using the AUC (area under the curve) measure [35], which corresponds to the probability that a randomly chosen species presence site has a higher occurrence probability than a randomly chosen background site [38]. The two MaxEnt models selected have AUC values of 0.894 (*Balanus crenatus*) and 0.885 (*Cancer pagurus*). A value of 0.5 indicates a model that is no better than random, while 0.75 and above is taken as useful [57]. Values between 0.8 and 0.9 indicate a good prediction [58]. In both cases, 75% of the data is used to train the model and 25% is randomly held back to test it. The test data is shown to fit well with the models, with test AUCs of 0.870 and 0.856 respectively.

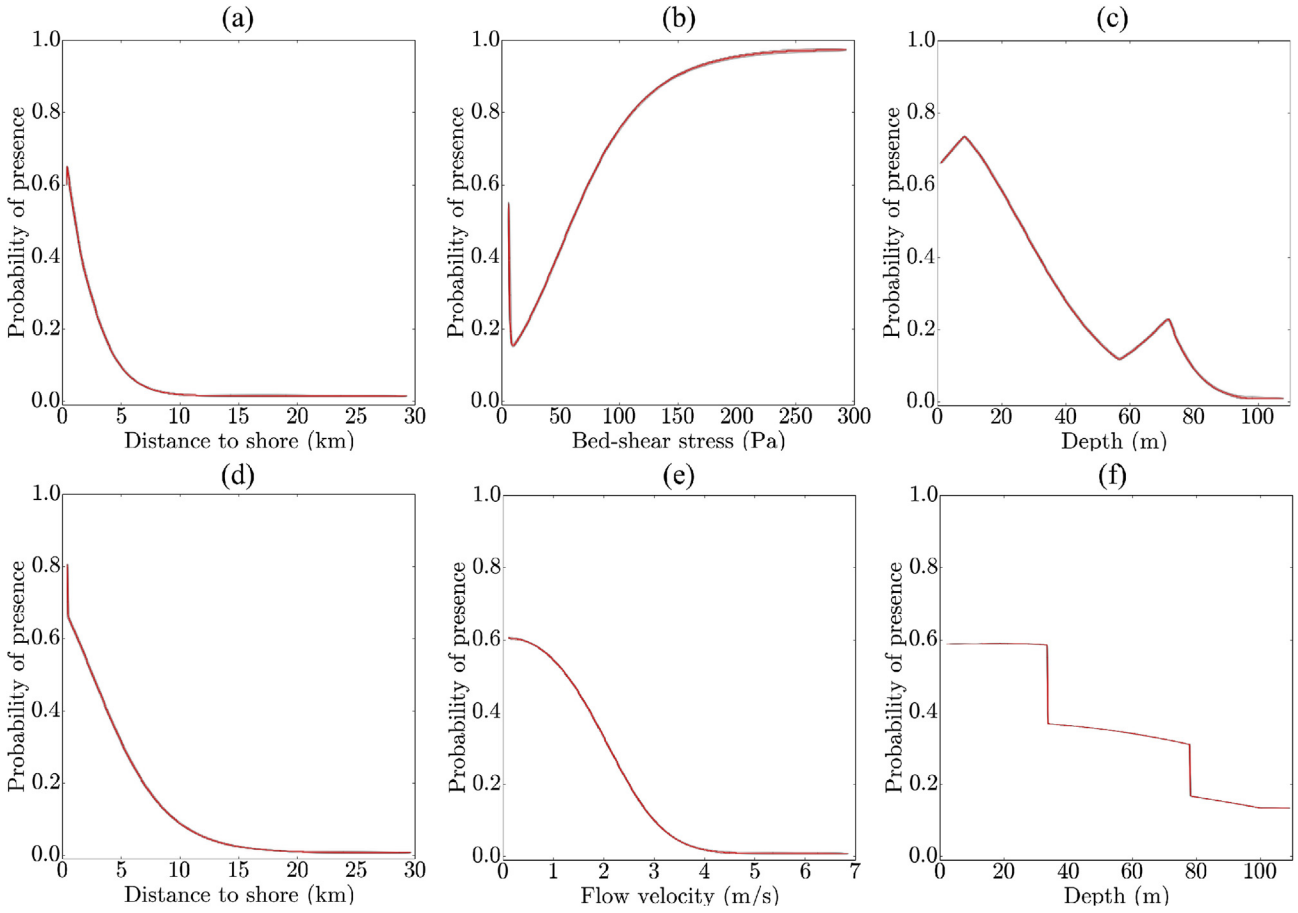

Fig. 4. Comparison of response curves of the most important environmental variables for the species distribution of *Balanus crenatus* - a) distance to shore, b) bed shear stress and c) depth, and *Cancer pagurus* - d) distance to shore e) flow velocity and f) depth. Response curves give information on the dependance of habitat suitability on each environmental variable, although they do not completely capture this relationship, missing, for example, the relationships between environmental variables.

For each species, the vector λ is output by Maxent and read into OpenTidalFarm, and a habitat functional is created for that species, as described in section 3.2. This gives OpenTidalFarm the ability to optimise for habitat suitability, H, of either *Cancer pagurus* or *Balanus crenatus*. The exploration of the Pareto front can now continue as described in section 3.3.

5. Results

5.1. Initial optimisation

OpenTidalFarm is initially run to optimise for profit alone. This produces arrays that generate the maximum possible profit in the given environment (Fig. 5). Given that this simulation set-up recreates peak flood flow only, the arrays are larger and produce more power, and more profit, than arrays we might expect to see built in these locations. For results where the forward model is run over the entire tidal cycle see Funke et al. [25].

The optimal designs of the four farms vary quite significantly, as the characteristics of each site are different. There are, however, still similarities across the farms in that turbines tend to be grouped together in barrages that are aligned perpendicular to the flow, as demonstrated in Funke et al. [25] through the visualisation of streamlines. The optimised array designs observed for farms 3 and 4 preferentially deploy turbines in the same locations as was found in Ref. [25], namely the eastern and western sides of the northern half of farm 3 and the south-western boundary of farm 4. Farms 1 and 2 show the characteristic barrage like structures that were observed in Ref. [25], but additionally show a tendency to deploy turbines along the site boundaries aligned with the flow direction. This feature can be seen more clearly in Fig. 6, and can be explained through two factors. In the case of farm 1 the band of high turbine

Fig. 5. Optimised array designs for Farms 1–4.

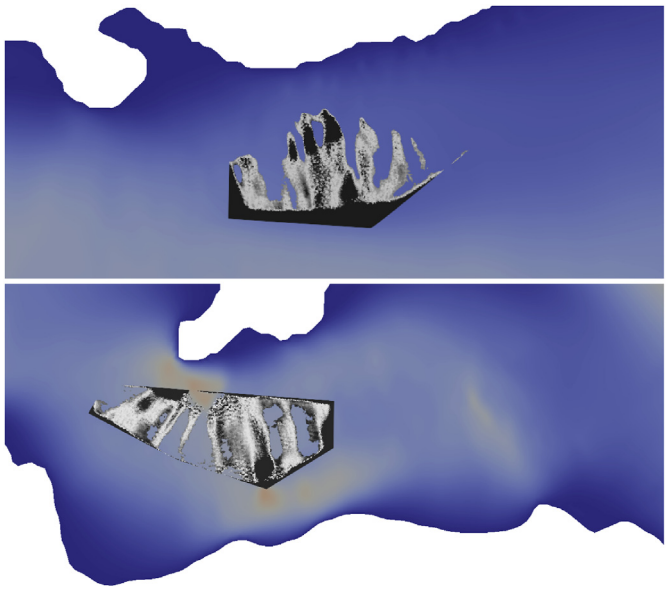

Fig. 6. Close up view of Farms 1 (top) and 2 (bottom) with the colour field showing the flow velocity and the grey scale showing the turbine concentration. (For interpretation of the references to colour in this figure legend, the reader is referred to the Web version of this article.)

concentration which only occurs to the south corresponds to regions of high background velocity, as seen in Figs. 2(a) and 6, which are a consequence of the local bathymetry and location of the landmass to the north. For farm 2, additional channel scale blockage effects lead to accelerated bypass flow to the immediate north and south of the array; this has the effect of encouraging the placement of turbines close to these regions along the northern and southern borders of the farm. This accelerated bypass flow can clearly be seen in Fig. 7(c). Note that this feature, along with the open nature of the western boundary (the 'inflow' in this flood only case), has agreement with the optimised array designs obtained for this site using a discrete turbine approach in Ref. [8]. Later in Fig. 9 turbines will be seen to be removed from the northern and southern borders of farm 2, while barrage-like structures remain, as the weighting of the habitat functional relative to the profit functional is increased resulting in a reduction of these strong channel-scale bypass flows.

As can be seen from Table 1, farms 1 and 2 produce many times more power than farms 3 and 4 due to their much higher numbers of turbines. However, when you compare farms 1 and 2 to each other, farm 2 produces more than twice the power of farm 1 despite having less than half the turbines. This is due to the farms situation in much faster-flowing water. In contrast to this, most of Farm 4 lies empty as the flow velocities through it are too low for turbines to be profitable. Such difference in the design and situation of each farm shows that this scenario is well suited to test out how the habitat functional will work under different conditions.

Table 1
Optimised properties of the four tidal farms.

	Farm 1	Farm 2	Farm 3	Farm 4
Profit (MW)	539	1699	313	132
Power (MW)	782	1804	565	160
Cost (MW)	243	105	25	28
No. Turbines	1586	687	165	182

Specific results of the following two test cases should be considered with caution. These test cases were chosen not because of scientific or public interest in the species, and they exist only to demonstrate that the methods presented can be used to identify the effects of proposed tidal farms on a range of species or habitats, and to design arrays that protect, or even increase, the suitability of those habitats.

5.2. *Balanus crenatus*

The optimisation is run with the two opposing functionals of profit, P, and habitat suitability of *Balanus crenatus*, H. ι is increased from 0 until profit falls close to zero. Habitat suitability is measured by integrating occurrence probability across the entire domain. Optimisations converged in an average of 36 iterations.

Without the presence of any tidal arrays, the occurrence probability is highest in the centre of the Firth where the flow between the islands causes the bed shear stress to be high, and where proximity to those islands also causes distance to shore to be low. In these locations, near both farms 2 and 3, occurrence probability lies around 70% (Fig. 7 (a)). Near the coastlines where distance to shore is low but the water flows more slowly, reducing bed shear stress, occurrence probability falls to around 50%, and in areas that are too deep, or too far from shore, occurrence probability drops to 20% or below.

The introduction of the four farms optimised for power alone can be seen to alter habitat suitability in the region (Fig. 7 (b)). Through the northern channel of the Pentland Firth (covering Farm 1 and passing by Farm 4) occurrence probability drops by 5–10%, while in the southern channel containing Farms 2 and 3, the Inner Sound of Stroma, this fall is as high as 40%. The primary reason for

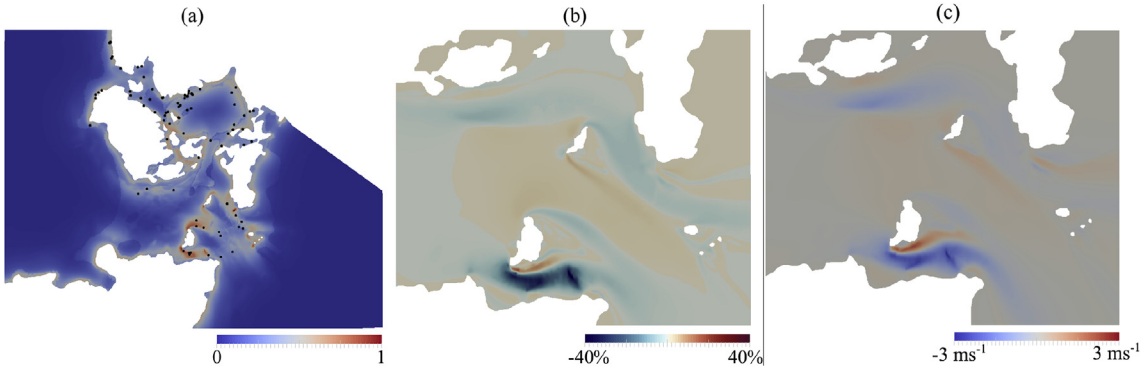

Fig. 7. (a) Species occurrence probability for *Balanus crenatus*, with species presence points marked in black, (b) change in occurrence probability under the influence of arrays optimised for P only (i.e. $\iota = 0$), and (c) the change in tidal velocity due to the presence of the same array.

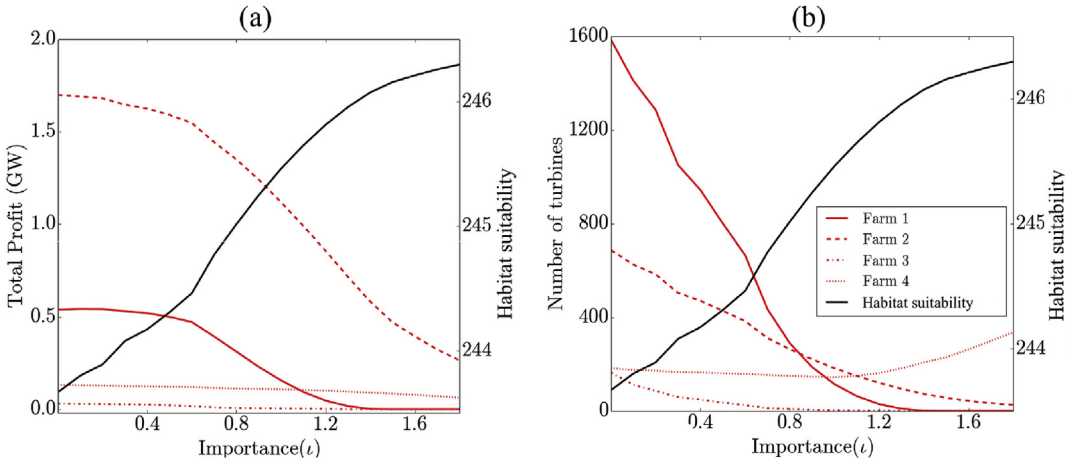

Fig. 8. (a) profit and (b) number of turbines for each of the four farms in the Pentland Firth for increasing ι. Plotted against habitat suitability, measured by integrating the occurrence probability function across the entire domain.

this is the drop in bed shear stress in these regions that comes with the removal of energy from the tidal stream. There are small areas where occurrence probability is increased, due to jets of faster flowing water being diverted around the new arrays, or around islands. This is most pronounced between the north of Farm 2 and the south coast of Stroma but even in this small area the increase is only by up to 10%.

As ι is increased the number of turbines in each farm falls (Fig. 8

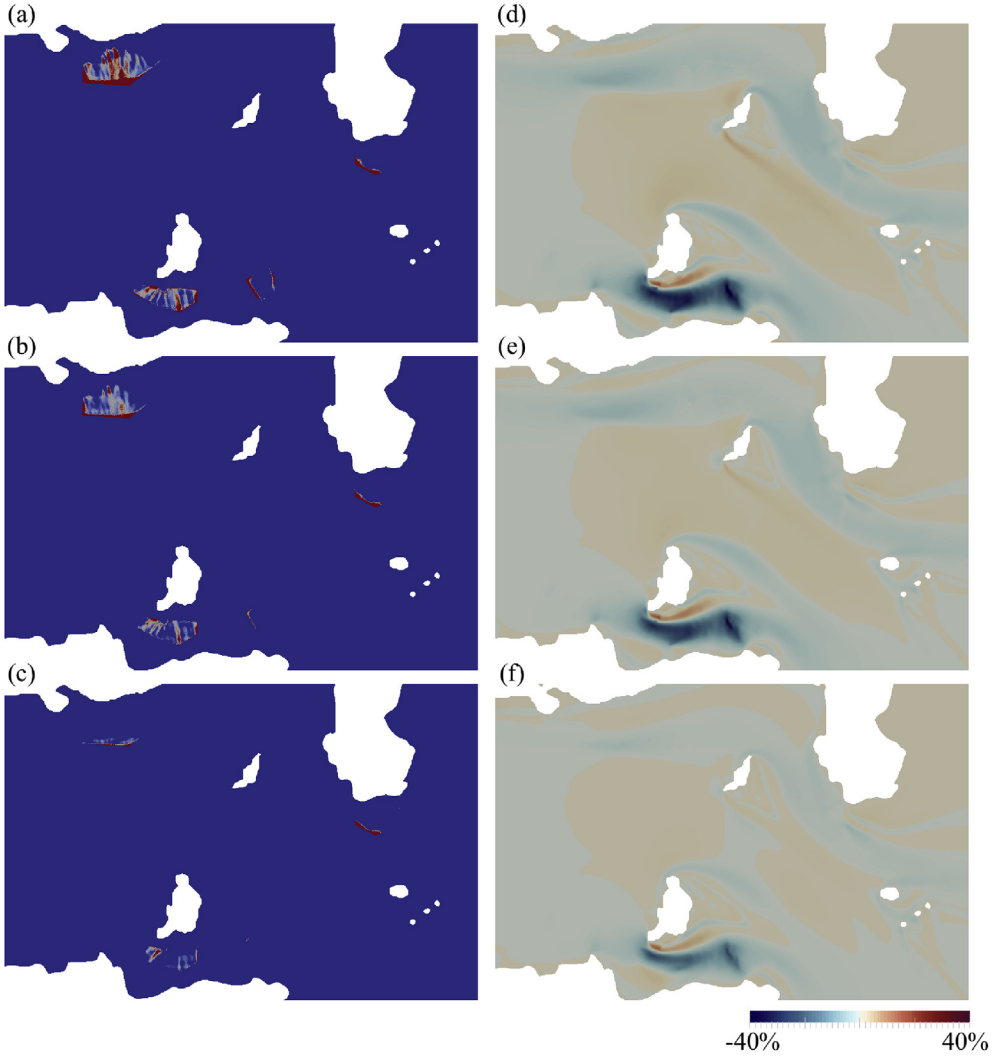

Fig. 9. Optimised turbine arrays for ι (a) 0, (b) 0.5, and (c) 1. Effect on occurrence probability by optimised arrays with ι (d) 0, (e) 0.5, and (f) 1.

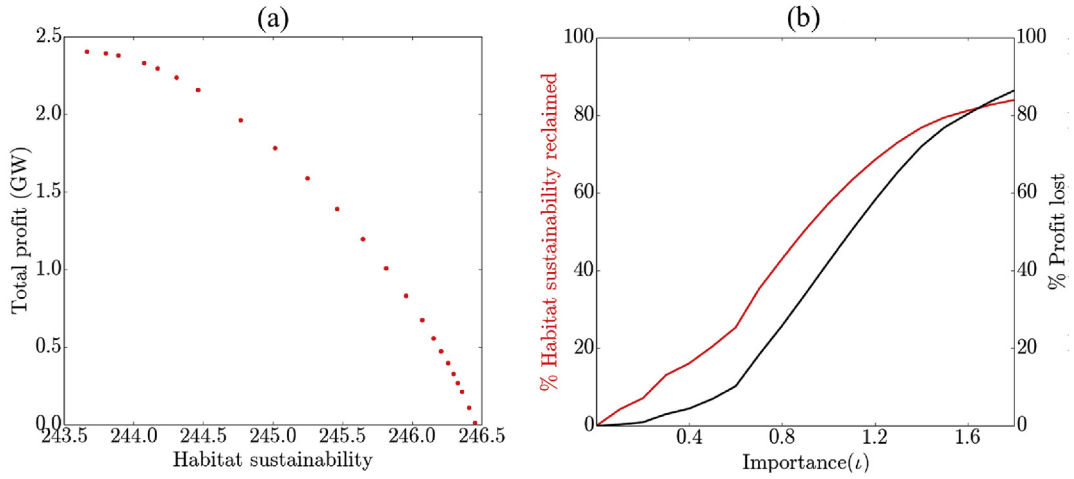

Fig. 10. (a) Points on the Pareto front for ι values of 0–2.3. (b) Percentage changes in Habitat suitability and Profit for ι increasing from 0 to 2.3. Both graphs from the *Balanus crenatus* demonstration scenario.

(b)). The larger farms, particularly Farm 1, lose turbines at the fastest rate. Farm 4, unlike the others, retains its turbines, and when ι rises high enough more turbines are added. These turbines are a result of an over-inflated ι value, to the point that the generation of profit no longer matters, and this anomaly can be discarded. These turbines produce no profit, and are only put in place to increase blockage around a headland resulting in an increase in flow velocity, and therefore bed shear stress, around that point. The general loss in turbines reflects that *Balanus crenatus* prefers higher bed shear stress, and the presence of turbines necessarily slows the flow and reduces bed shear stress. With this drop in turbine number comes a corresponding loss in profit (Fig. 8 (a)). This loss is initially quite small, with little difference made to the profit of farms despite the rapidly falling turbine numbers. This is for two reasons. Firstly, many turbines, particularly in Farm 1 which is in slower flowing water, will be producing minimal profit, and these turbines are removed first. Secondly, the reduction in the number of turbines (that can be seen in Fig. 9) also reduces blockage effects across the farm domains, increasing the flow through them, resulting in each turbine producing more power. This shows that the optimisation process is successful, making gains to habitat suitability with as low an impact on profit as possible.

The Pareto front for this problem is found by performing the optimisation with a series of ι values (Fig. 10 (a)). Each Pareto point represents the final solution to the optimisation for a value of ι between 0 and 2.5. As ι rises the Pareto front curves from high P low H to low P high H, demonstrating the efficacy of the technique. In previous work where the turbines were represented discretely, fixing turbine number and thus over-constraining the solution space [22], the Pareto front was convex in places and hard to uncover. With the continuous approach, the Pareto front is smooth and concave and a relationship between the size of the development and the corresponding effects on habitat suitability can be identified. To demonstrate this, loss in profit is plotted against the reclaimed habitat suitability as ι rises (Fig. 10 (b)). Here the nature of the trade-off becomes apparent, and it is seen that to a certain degree habitat suitability can be improved without a large impact on profit. For example, at an ι value of 0.4, habitat suitability regains 16% of its loss at a cost of 4% of overall profit. Which of these is more valuable however can only be decided by stakeholders in the arrays themselves.

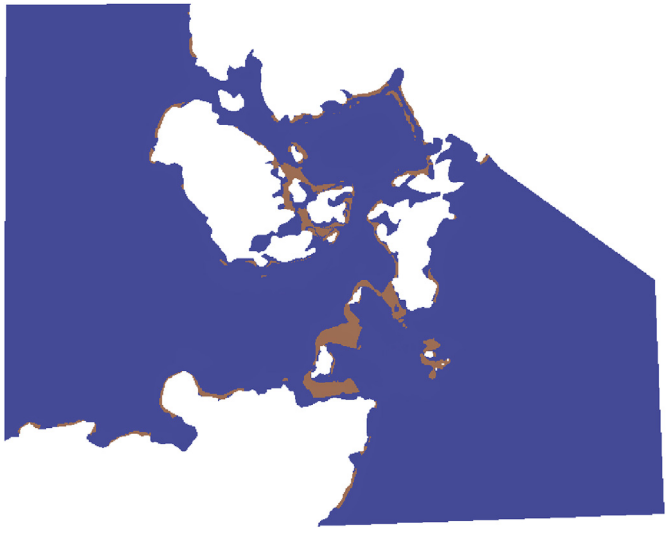

Fig. 11. Areas where occurrence probability of *Balanus crenatus* is greater than 0.6.

5.3. *Balanus crenatus*: preferred habitat

There are areas in the domain, particularly around Farm 1, where the habitat functional causes profit to be lost in order to gain what could be seen as a 'wasted' increase is occurrence probability. That is, the gain is minimal and in an area where occurrence probability is always going to remain low because, for example, it is too deep. To combat this effect the simulations are repeated with the Habitat functional applied only to areas of occurrence probability greater than 0.6 (Fig. 11), a value used in literature to be a threshold of 'high' habitat suitability [59,60]. These areas are referred to as *preferred habitat*.

This change has a significant effect on the optimal array formations, sizes and profits (Figs. 12 and 13). Farm 2, which lies entirely in preferred habitat, shows a drop in turbine numbers and profit as before. Farms 1 and 4 which lie outside of preferred habitat do not change significantly. Farm 3 bridges the edge of the preferred habitat and it can be seen to shift all of its turbines to lie outside of this zone. Also, due to the loss of turbines in Farm 2 increasing flow through the southern channel, Farm 3 is able to increase the total number of turbines it contains and generate more power and profit (Fig. 13), without negatively affecting any of the

Fig. 12. Optimised turbine arrays for ι (a) 0.5, (b) 1, with the habitat functional applied only to areas with occurrence probability greater than 0.6.

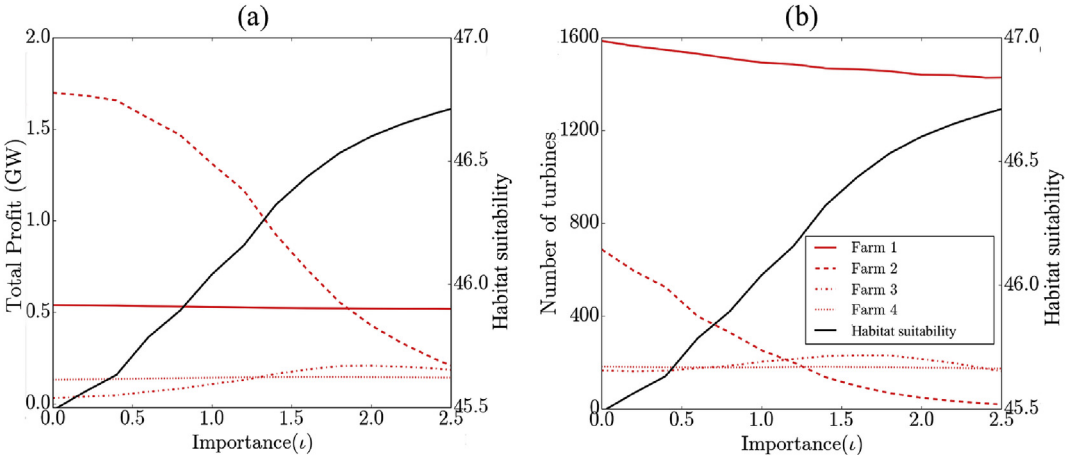

Fig. 13. (a) profit and (b) number of turbines for each of the four farms in the Pentland Firth for increasing ι, with the habitat functional applied only to areas with occurrence probability greater than 0.6.

areas of preferred habitat.

5.4. *Cancer pagurus*

This time the optimisation is run with the two opposing functionals of profit, P, and habitat suitability of *Cancer pagurus*, H. ι increased is from 0 until profit falls close to zero. As before, habitat suitability is measured by integrating occurrence probability across the entire domain. Optimisations converged in an average of 34 iterations.

Fig. 14 (a) shows that throughout most of the domain the occurrence probability of *Cancer pagurus* lies between 5% and 10%, rising to between 50% and 70% in shallow waters (< 35 m) and coastal regions, as long as the flow velocity does not go far beyond 3

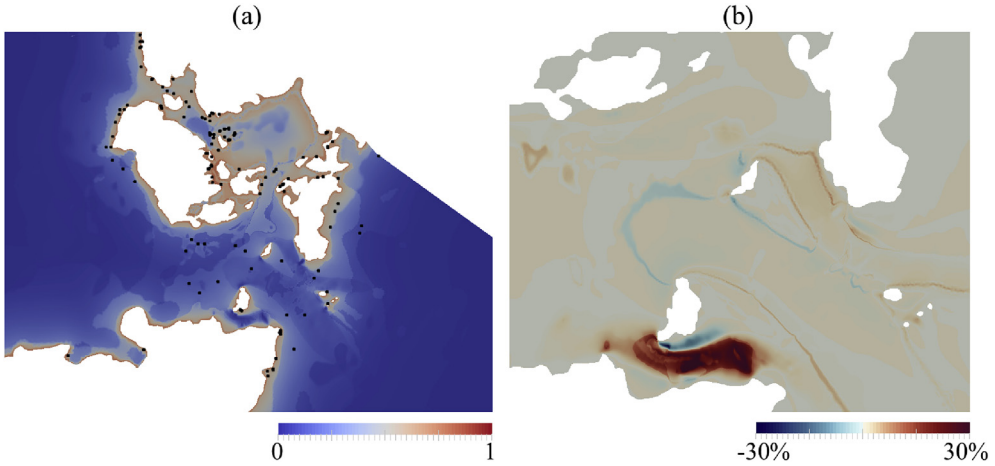

Fig. 14. (a) Species occurrence probability for *Cancer pagurus*, with species presence points marked in black, and (b), and change in occurrence probability under the influence of arrays optimised for power alone ($\iota = 0$).

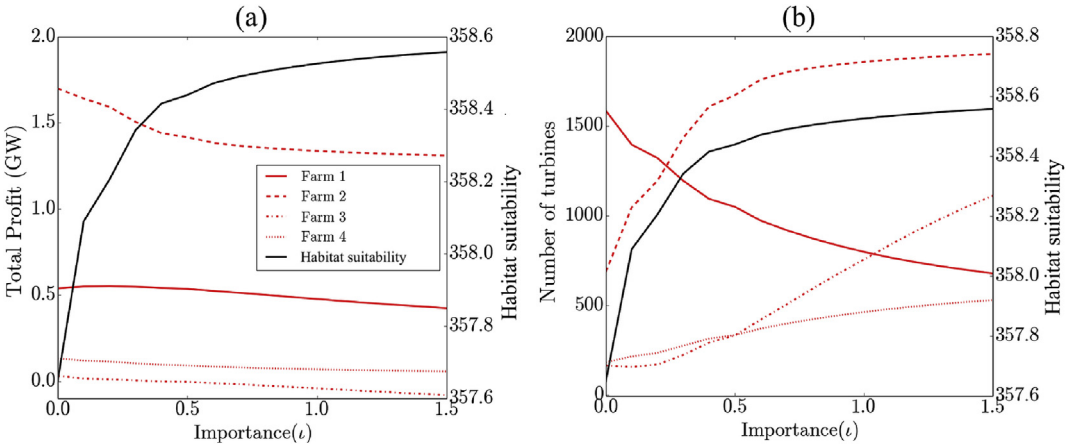

Fig. 15. (a) profit, and (b) number of turbines for each of the four farms in the Pentland Firth for increasing ι. Plotted against 'habitat suitability', measured by integrating the occurrence probability function across the entire domain.

m s^{-1}. The introduction of the four tidal farms has a minimal effect on occurrence probability across most of the domain, indeed it is only in the vicinity of Farms 2 and 3 where much change is seen (Fig. 14 (b)), and occurrence probability rises by up to 30%. The reason for this is that Farms 2 and 3 are in a unique position within this domain of being in a channel that is shallow enough to support a high occurrence probability, but one that does not because the flow through it is too fast. The introduction of the two tidal farms slows the current through this channel thus making it suitable for habitation. Farms 1 and 4 have little impact on habitat suitability as the water the turbines are situated in is too deep, so their effects on the flow go unnoticed by the species.

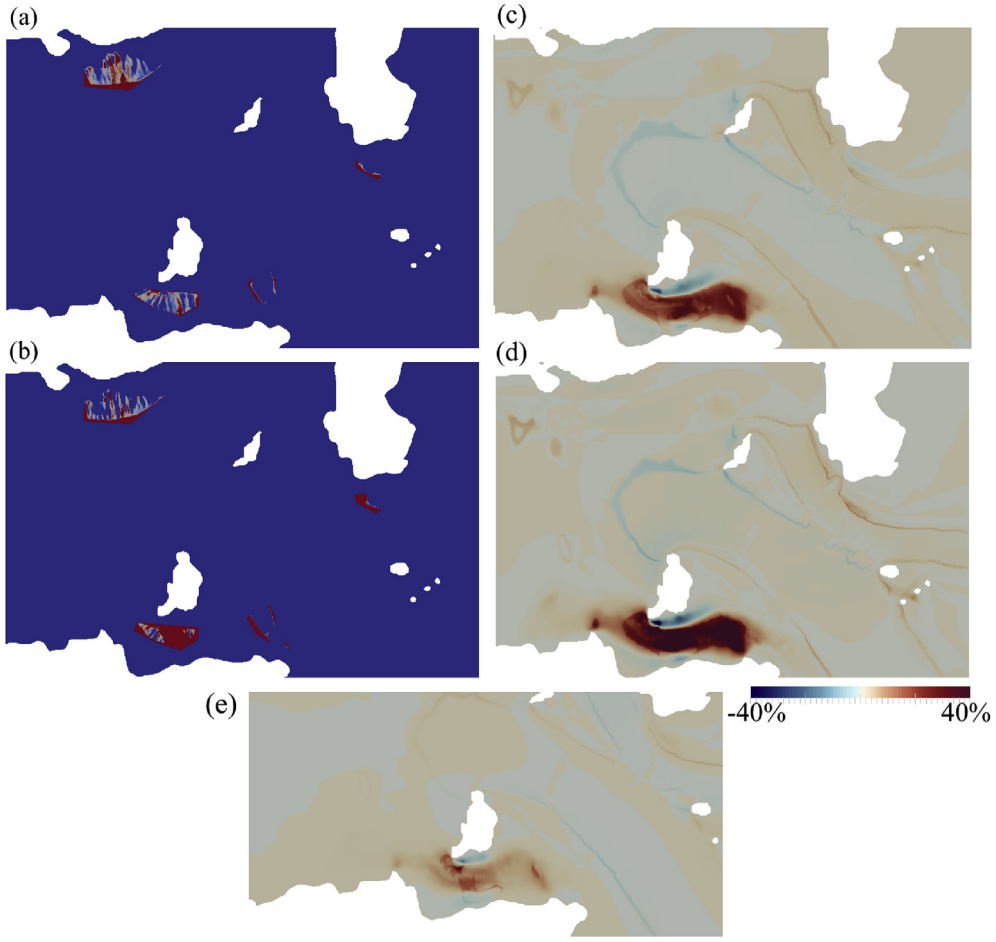

Fig. 16. Optimised turbine arrays for ι (a) 0 and (b) 0.5. Effect on occurrence probability by optimised arrays with ι (c) 0 and (d) 0.5. (e) shows the difference between plots (c) and (d).

As ι is increased the four farms act in different ways (Figs. 15 and 16). Turbines gain dual purpose, of both generating power and slowing down flow that is inhibiting habitat suitability. The higher ι is, the more important the second objective becomes. This results in turbines located in already slow flowing water being dropped as they contribute least to power and are not necessary to increase occurrence probability. As a result Farm 1 again loses turbines swiftly (Fig. 15 (b)), starting with those where the currents are weakest and that generate the least power. As before the corresponding drop in profit is much more gradual (Fig. 15 (a)). Farms 2 and 3 gain turbines rapidly in an attempt to staunch the flow through the Inner Sound of Stroma further, and thus increase habitat suitability even more. The blockage effects of these additional turbines are such that the power generated by the farm falls, and the profit of course follows.

The overall result on habitat suitability can be seen in Fig. 16, with a further increase of occurrence probability in the Inner Sound of Stroma, rising to a 40% increase at $\iota = 0.5$, with little change beyond that point. The Pareto front is again plotted for ι increasing from 0 to 2 (Fig. 17) and again it is smooth and its shape easy to find. This shows that we are successfully identifying the best solutions to improve habitat suitability with minimal impact on profit.

6. Discussion and conclusions

The Habitat functional introduced into OpenTidalFarm has proven to be both easy to use and effective in achieving results. OpenTidalFarm itself is ideally suited to finding Pareto optimal solutions to the multi-objective optimisation problem posed, doing so in an average of 35 iterations. Using the continuous turbine approach it is found that the Pareto front is concave and easy to navigate, unlike in previous work where turbines were expressed discretely and thus the number of turbine present in an array had to be fixed a-priori. This both reduces the number of iterations required to find each optimal solution and simplifies the exploratory process thus reducing the number of optimisations required to map the Pareto front. From examining the Pareto fronts of the two test cases (Figs. 10 and 17) relationships between the opposing goals of profit generation and habitat suitability are successfully identified, and information is gathered on the trade-offs that exist for these species.

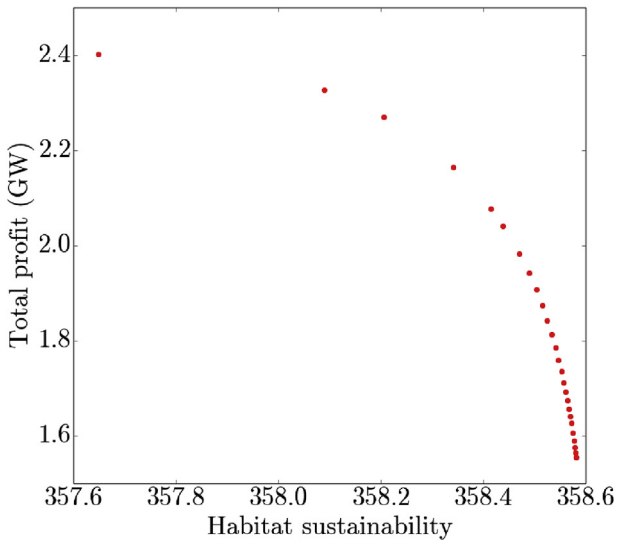

Fig. 17. Points on the Pareto front, for ι values of 0–2, from the *Cancer pagurus* demonstration scenario.

The possible impacts that proposed tidal developments could have on marine habitats are commonly discussed [6,16,61], as was recently well summarised by Gallego et al. [62]. This work represents an early attempt at demonstrating how impacts could be explicitly quantified, modelled and potentially minimised, in the specific case of changing hydrodynamics impacting on specific habitats. The use of a steady-state hydrodynamic model introduces caveats in the accuracy of the environmental data being fed into the habitat suitability model, so specific results should be considered insofar as they prove the concept of the approach detailed; an approach that is additionally novel in that it includes the environmental effects of a turbine array in its own array design process, altering array design to reduce negative effects, or increase positive ones.

With greater time allowances these methods could be extended to time-dependent problems where the hydrodynamic model covers multiple tidal cycles. Indeed if this method was being implemented to inform a decision on array design this approach should certainly be taken. As well as being necessary to model the environment accurately, this would allow for the inclusion of further environmental variables in the MaxEnt model, such as tidal asymmetry.

The two example test cases considered in this work demonstrate that different species will react in potentially vastly different ways to the introduction of tidal turbine arrays. Depending on the species, there could be a positive influence, negative influence, or no influence at all. Similarly, even when just looking at one species, each of the four farms had different effects and so reacted in different ways to the increased importance of habitat suitability. This highlights the uncertainty and complexity that exists around the environmental effects of such development and demonstrates the need for in-depth studies of potential effects around any planned tidal development. There is, however, some reassurance that the regional effects of the four tidal farms were generally small, with large impacts on species occurrence happening almost entirely in and around the farms themselves.

The methods employed here can be used to examine the effects tidal developments could have on scientifically or socially significant species or, by using a set of indicator species, on specific habitat types. This could allow for a complete review of the impacts of a planned tidal development that looks at the potential effects on all species of interest in the area, and how the arrays might be built to mitigate these effects. This could help to ensure the protection of endangered species, or important breeding grounds or nurseries in the area, with functionals for different species applied to different locations. The information gathered from such an investigation, such as the relationships and trade-offs discovered between habitat suitability and profit, could then be examined by stakeholders in the construction of the array in order to inform decisions that must be made on array design.

Acknowledgements

The authors would like to acknowledge Imperial College London's Earth Science and Engineering department, and the Natural Environment Research Council for a Doctoral Training Partnership scholarship awarded through the Grantham Institute for Climate Change, as well asEPSRC grants (EP/J010065/1, EP/M011054/1), for providing the funding that supported this work.

References

[1] S.J. Couch, I. Bryden, Tidal current energy extraction: hydrodynamic resource characteristics, J. Eng. Mar. Environ. 220 (2006) 185–194.
[2] I. Bryden, S. Couch, A. Melville, Tidal current resource assessment, Proc. IME J.

Power Energy 221 (2007) 125–135.
[3] S. Draper, T.A.A. Adcock, A.G.L. Borthwick, G.T. Houlsby, Estimate of the tidal stream power resource of the Pentland Firth, Renew. Energy 63 (2014) 650–657.
[4] T.A.A. Adcock, S. Draper, G.T. Houlsby, A.G.L. Borthwick, S. Serhadlıoğlu, The available power from tidal stream turbines in the Pentland Firth, Proc. Roy. Soc. Lond.: Math. Phys. Eng. Sci. 469 (2157) (2013).
[5] R. Martin-Short, J. Hill, S.C. Kramer, A. Avdis, P.A. Allison, M.D. Piggott, Tidal resource extraction in the Pentland Firth, UK: potential impacts on flow regime and sediment transport in the Inner Sound of Stroma, Renew. Energy 76 (2013) 596–607.
[6] M.A. Shields, D.K. Woolf, E.P.M. Grist, S.A. Kerr, A.C. Jackson, R.E. Harris, M.C. Bell, R. Beharie, A. Want, E. Osalusi, S.W. Gibb, J. Side, Marine renewable energy: the ecological implications of altering the hydrodynamics of the marine environment, Ocean Coast Manag. 54 (2011) 2–9.
[7] M.A. Shields, L.J. Dillon, D.K. Woolf, A.T. Ford, Strategic priorities for assessing ecological impacts of marine renewable energy devices in the Pentland Firth (Scotland, UK), Mar. Pol. 33 (2009) 635–642.
[8] S.W. Funke, P.E. Farrell, M.D. Piggott, Tidal turbine array optimisation using the adjoint approach, Renew. Energy 63 (2014) 658–673.
[9] R. Ahmadian, R.A. Falconer, Assessment of array shape of tidal stream turbines on hydro-environmental impacts and power output, Renew. Energy 44 (2012) 318–327.
[10] S.E. Ben Elghali, M.E.H. Benbouzid, J.F. Charpentier, Marine tidal current electric power generation technology: state of the art and current status, in: IEEE IEMDC'07, vol. 2, Antalya, Turkey, May 2007, pp. 1407–1412.
[11] C. Garret, P. Cummins, The power potential of tidal currents in channels, Proc. Math. Phys. Eng. Sci. 461 (2005).
[12] ABP Mer, Quantification of Exploitable Tidal Energy Resources in the UK, Technical report, ABP Marine Environmental Research Ltd, 2007.
[13] S. Baston, S. Waldman, J. Side, Modelling Energy Extraction in Tidal Flows, Technical report, TeraWatt Consortium, 2014.
[14] D.M. Culley, S.W. Funke, S.C. Kramer, M.D. Piggott, A hierarchy of approaches for the optimal design of tidal turbine arrays, in: Proc. Of ICOE 2014 (5th International Conference on Ocean Energy), 2014.
[15] Astrid Harendza, Benthic Habitats in a Tide-Swept Channel of the Pentland Firth and Their Potential Responses to a Tidal Energy Development, PhD thesis, Environmental Research Institute, University of Aberdeen, 2014.
[16] A.B. Gill, Offshore renewable energy: ecological implications of generating electricity in the costal zone, J. Appl. Ecol. 42 (2005) 605–615.
[17] B. Wilson, R.S. Batty, F. Daunt, C. Carter, Collision risks between marine renewable energy devices and mammals, fish and diving birds, Technical report, in: Report to the Scottish Executive, Scottish Association for Marine Science, 2006.
[18] L.S. Blunden, A.S. Bahaj, Effects of tidal energy extraction at Portland Bill, southern UK predicted from a numerical model, IMechE 221 (2007) 137–146.
[19] D. Fallon, M. Hartnett, A. Olbert, S. Nash, The effects of array configuration on the hydro-environmental impacts of tidal turbines, Renew. Energy 64 (2014) 10–25.
[20] J. van der Molen, P. Ruardij, N. Greenwood, Potential environmental impact of tidal energy extraction in the Pentland Firth at large spatial scales: results of a biogeochemical model, Biogeosciences 13 (2016) 2593–2609.
[21] D. Haverson, Numerical Modelling of the Interaction Between Tidal Stream Turbines and the Benthic Environment, PhD thesis, University of Exeter, 2017.
[22] R.J. du Feu, S.W. Funke, S.C. Kramer, D.M. Culley, J. Hill, B.S. Halpern, M.D. Piggott, The trade-off between tidal-turbine array yield and impact on flow: a multi-objective optimisation problem, Renew. Energy 114 (2017) 1247–1257.
[23] S.J. Phillips, M. Dudik, R.E. Schapire, MaxEnt Software for Modelling Species Niches and Distributions, 2018, version 3.4.1.
[24] S.W. Funke, OpenTidalFarm, 2016.
[25] S.W. Funke, S.C. Kramer, M.D. Piggott, Design optimisation and resource assessment for tidal-stream renewable energy farms using a new continuous turbine approach, Renew. Energy 99 (2016) 1046–1061.
[26] D.M. Culley, S.W. Funke, S.C. Kramer, M.D. Piggott, Integration of cost modelling within the micro-siting design optimisation of tidal turbine arrays, Renew. Energy 85 (2016) 215–227.
[27] R.H.J. Willden, T. Nishino, J. Schluntz, Tidal stream energy: designing for blockage, in: Proceedings of 3rd Oxford Tidal Energy Workshop, 2014, pp. 27–28.
[28] M. Bilbao, E. Alba, Simulated annealing for optimization of wind farm annual profit, in: 2009 2nd International Symposium on Logistics and Industrial Informatics, Sept 2009.
[29] S.J. Phillips, M. Dudik, R.E. Schapire, A maximum entropy approach to species distribution modeling, in: Proceedings of the Twenty-First International Conference on Machine Learning, 2004, pp. 655–662.
[30] E. Sanford, D. Bermudez, M.D. Bertness, S.D. Gaines, Flow, food supply and acorn barnacle population dynamics, Mar. Ecol. Prog. Ser. 104 (1994) 49–62.
[31] D.J. Crisp, Factors influencing growth rate in balunus balanoides, J. Anim. Ecol. 25 (1960) 95–116.
[32] MarLIN, Biotic - Biological Traits Information Catalogue, 2006.
[33] T.D. Nickell, P.G. Moore, The behavioural ecology of epibenthic scavenging invertebrates in the clyde sea area: laboratory experiments on attractions to bait in moving water, underwater tv observation in situ and general conclusions, J. Exp. Mar. Biol. Ecol. 159 (1992) 15–35.
[34] NBN, National Biodiversity Network Atlas Website, 2018.
[35] S.J. Phillips, R.P. Anderson, R.E. Schapire, Maximum entropy modeling of species geographic distributions, Ecol. Model. 190 (2006) 231–259.
[36] J. Elith, S.J. Phillips, T. Hastie, M. Dudik, Y. En Chee, C.J. Yates, A statistical explanation of maxent for ecologists, Divers. Distrib. 17 (2011) 43–57.
[37] C. Merow, M.J. Smith, J.A. Silander Jr., A practical guide to MaxEnt for modeling species' distributions: what it does, and why inputs and settings matter, Ecography 36 (2013) 1058–1069.
[38] S.J. Phillips, M. Dudik, Modeling of species distributions with MaxEnt: new extensions and a comprehensive evaluation, Ecography 31 (2008) 161–175.
[39] D.P. Tittensor, A.R. Baco, P.E. Brewin, M.R. Clark, M. Consalvey, J. Hall-Spencer, A.A. Rowden, T. Schlacher, K.I. Stocks, A.D. Rogers, Predicting global habitat suitability for stony corals on seamounts, J. Biogeogr. 36 (2009) 1111–1128.
[40] C. Merow, J.A. Silander Jr., A comparison of maxlike and maxent for modelling species distributions, Meth. Ecol. Evol. 5 (2014) 215–225.
[41] J. Elith, C.H. Graham, R.P. Anderson, M. Dudik, S. Ferrier, A. Guisan, R.J. Hijmans, F. Huettmann, J.R. Leathwick, A. Lehmann, J. Li, L.G. Lohmann, B.A. Loiselle, G. Manion, C. Moritz, M. Nakamura, Y. Nakazawa, J. McC. Overton, A. Townsend Peterson, S.J. Phillips, K. Richardson, R. Scachetti-Pereira, R.E. Schapire, J. Soberón, S. Williams, M.S. Wisz, N.E. Zimmermann, Novel methods improve prediction of species' distributions from occurrence data, Ecography 29 (2006) 129–151.
[42] J.M. Gonzlez-Irusta, M. Gonzalez-Porto, R. Sarralde, B. Arrese, B. Almn, P. Martn-Sosa, Comparing species distribution models: a case study of four deep sea urchin species, Hydrobiologia 745 (2015) 43–57.
[43] S. Della Pietra, V. Della Pietra, J. Lafferty, Inducing features of random fields, IEEE Trans. Pattern Anal. Mach. Intell. 19 (1997) 1–13.
[44] European Marine Observation and Data Network, 2018. http://www.emodnet-seabedhabitats.eu.
[45] European Environment Agency, European Nature Information System, eunis, 2018.
[46] K.V. Moffaert, M.M. Drugan, A. Nowe, Scalarized multi-objective reinforcement learning: novel design techniques, in: Proceedings of Adaptive Dynamic Programming and Reinforcement Learning, ADPRL), 2013, pp. 191–199.
[47] The Crown Estate, Pentland Firth and Orkney Waters Strategic Area Review, 2013.
[48] A. Avdis, A.S. Candy, J. Hill, S.C. Kramer, M.D. Piggott, Efficient unstructured mesh generation for marine renewable energy applications, Renew. Energy 116 (2018) 842–856.
[49] British Oceanographic Data Centre, UK Tide Gauge Network, 2018.
[50] Edina Digimap Service, Hydrospatial One, Gridded Bathymetry, 2017.
[51] Scottish Government, Pentland Firth Bathymetry, 2009.
[52] M.C. Easton, D.K. Woolf, S. Pans, An operational hydrodynamic model of a key tidal-energy site: inner sound of stroma, pentland firth (Scotland, UK), in: Proc. of the 3rd International Conference on Ocean Energy, 2010.
[53] Susana Baston, Robert Ewan Harris, Modelling the hydrodynamic characteristics of tidal flow in the pentland firth, in: Proceedings of 9th European Wave and Tidal Energy Conference, 2011.
[54] M.C. Easton, D.K. Woolf, The dynamics of an energetic tidal channel, the Pentland Firth, Scotland, Cont. Shelf Res. 48 (2012) 50–60.
[55] M.A. Hemmer, The magnitude and frequency of combined flow bed shear stress as a measure of exposure on the australian continental shelf, Cont. Shelf Res. 26 (2006) 1258–1280.
[56] M.C. Bell, E.P.M. Grist, S. Baston, S. Rouse, M. Spencer Jones, J.S. Porter, A. Want, R.E.H., J.C. Side, Hydrokinetic energy as an ecological factor – how might wave and tidal energy extraction affect the distribution of marine organisms?, in: ICES Annual Science Conference, 2011.
[57] J. Elith, Quantitative Methods for Modeling Species Habitat: Comparative Performance and an Application to Australian Plants, Springer, New York, 2000, pp. 39–58.
[58] D.W. Hosmer, S. Lemeshow, Applied Logistic Regression. Wiley Series in Probability and Statistics: Applied Logistic Regression, Wiley, New York, US, 2013.
[59] Sunil Kumar, Thomas Stohlgren, Maxent modeling for predicting suitable habitat for threatened and endangered tree canacomyrica monticola in New Caledonia, J. Ecol. Nat. Environ. 1 (08) (2009) 94–98.
[60] X. Yang, S.P.S. Kushwaha, S. Saran, J. Xu, P.S. Roy, Maxent modeling for predicting the potential distribution of medicinal plant, Justicia adhatoda L. in Lesser Himalayan foothills, Ecol. Eng. 51 (2013) 83–87.
[61] R. Inger, M.J. Attrill, S. Bearhop, A.C. Broderick, W.J. Grecian, D.J. Hodgson, C. Mills, E. Sheehan, S.C. Votier, M.J. Witt, B.J. Godley, Marine renewable energy: potential benefits to biodiversity? An urgent call for research, J. Appl. Ecol. 46 (2009) 1145–1153.
[62] A. Gallego, J. Side, S. Baston, S. Waldman, M. Bell, M. James, I. Davies, R. O'Hara Murray, M. Heath, A. Sabatino, D. McKee, C. McCaig, H. Karunarathna, I. Fairley, A. Chatzirodou, V. Venugopal, R. Nemalidinne, T.Z. Yung, A. Vgler, R. MacIver, M. Burrows, Large scale three-dimensional modelling for wave and tidal energy resource and environmental impact: methodologies for quantifying acceptable thresholds for sustainable exploitation, Ocean Coast Manag. 147 (2017) 67–77. Tools for managing the development of the wave and tidal energy resource (TeraWatt).